



Article

Mechanical Properties of Ballastless Track Considering Freeze–Thaw Deterioration Damage

Haoran Xie ^{1,2} , Lingyan Xu ^{1,2} and Bin Yan ^{2,3,*} ¹ China Railway Design Corporation, Tianjin 300308, China; xiehaoran@crdc.com (H.X.); xulingyan@crdc.com (L.X.)² School of Civil Engineering, Central South University, Changsha 410075, China³ National Engineering Research Center of High-Speed Railway Construction Technology, Changsha 410075, China

* Correspondence: binyan@csu.edu.cn

Abstract: In order to investigate the stress characteristics of ballastless track under high latitude, and multi-source and multi-field extreme temperature conditions. Based on the finite element theory and the elastic foundation beam–plate principle, a finite element model of the ballastless track considering the limit convex abutment, gel resin, and interlayer bonding is established. The mechanical characteristics of the ballastless track under the slab–CAM layer bonding state, mortar separation, freeze–thaw degradation and forced deformation of the foundation are studied. Considering the deterioration of materials, the bending moment and reinforcement of track structures in cold regions are checked and calculated. The studies show that under the action of negative temperature gradient load, the edge of the track slab is subjected to tension, and structural separation occurs at the edge of the slab. When the interface between the track slab–CAM layer is poorly bonded, the bearing capacity can be improved, and the amount of separation can be reduced by increasing the structural stiffness of the CAM layer. Under the action of freeze–thaw cycles, the material performance deteriorates seriously, the separation between the track structures intensifies, the baseplate is seriously powdered and cracked, and the maximum tensile stress exceeds 6 MPa. The CAM layer and the baseplate are weak structures, and the foundation frost heave occurs at the expansion joint of the baseplate, which is the frost heave condition. Under freeze–thaw deterioration, the original reinforcement design of the substructure structure does not meet the requirements of structural cracks and reinforcement yield stress. In severely cold areas, the structural reinforcement scheme should be reasonably determined.

Keywords: ballastless track; temperature load; freeze–thaw cycles; interface crack; reinforcement calculation

MSC: 65-11

Citation: Xie, H.; Xu, L.; Yan, B. Mechanical Properties of Ballastless Track Considering Freeze–Thaw Deterioration Damage. *Mathematics* **2023**, *11*, 2289. <https://doi.org/10.3390/math11102289>

Academic Editor: Gaohui Wang

Received: 9 April 2023

Revised: 6 May 2023

Accepted: 10 May 2023

Published: 14 May 2023



Copyright: © 2023 by the authors. Licensee MDPI, Basel, Switzerland. This article is an open access article distributed under the terms and conditions of the Creative Commons Attribution (CC BY) license (<https://creativecommons.org/licenses/by/4.0/>).

1. Introduction

Ballastless tracks are different from ballasted tracks; in addition to providing track elasticity, cushioning and shock absorption, the reinforced concrete structure has strong integrity, which can greatly reduce the accumulation of residual deformation in the track structure and maintain uniform stiffness [1,2]. Considering the construction characteristics and construction techniques used in track structures, under extreme temperature conditions such as those in extreme climate areas and subgrade frost heave and thawing areas, prefabricated slab unit ballastless track structures with low interoperability are often used to reduce the potential damage to the track structure under extreme load conditions. Climatic disasters such as seasonal frozen soil, upper arch, moisture, and differences in temperature may occur in regions with extreme climates. Scholars have conducted extensive and in-depth research on the stress damage law of ballastless track in cold regions, including the transition section of subgrades and bridges [3], the sunny side and shady

side of track structures [4,5], etc. The influence of temperature load [6], train load [7,8], foundation deformation [9], and other external factors on the mechanical properties of track systems have been studied. Zeng, ZP et al. [10] used the finite element software ABAQUS to establish a temperature field analysis model for a double-block ballastless track on the basis of test data, solar radiation theory and boundary heat transfer theory, and studied the influence of different routes and geographical latitudes on the temperature field. Dai Gonglian et al. [11] used the non-thickness interface bonding element to simulate the bonding contact force between the track plate and the mortar layer. Considering the interface bonding strength, interface shear load, and damage range of the track plate and the mortar layer, the failure mechanism of interface between the slab and the ballastless track was discussed; it was proved that the blade load at the edge of track plate and the mortar plate was the largest, and gradually decreased to the interior. Jiang, HG et al. [12] established a three-dimensional finite element model considering the contact between different layers in order to be able to simulate different settlement scenarios. The numerical results were verified by comparing the rail deflection with the full-scale physical model test. A unified formula for settlement amplitude and equivalent track flexibility was proposed to describe the geometric mapping relationship.

In view of the extremely prominent problems of material damage due to freeze–thaw cycles and the impact on the bonding state of subgrade thawing and frost heave under extreme temperature load in cold regions, the currently available studies related to the smoothness and mechanical characteristics of ballastless tracks on subgrades are still insufficient, and there is still relatively little research on the damage and deterioration of track structures under the coupling effect of subgrade freeze–thaw cycles and frost heave. Primarily, the stress checking of ballastless track structures does not take into account the impact of reductions in material properties. It is necessary to study the interaction damage characteristics of ballastless tracks in cold regions at high latitudes.

Due to the relatively limited amount of research performed by domestic and foreign scholars on the damage to and deterioration of track structures under the coupling effect of roadbed freeze–thaw cycles and frost heave, the performance reduction state of concrete materials is still unclear. In this paper, a nonlinear refined finite element model considering the limiting stop boss, annular gel resin, and interlayer bonding contact characteristics of a ballastless track on a subgrade is established to investigate the mechanical characteristics of ballastless tracks under multi-source and multi-field coupling effects. These include the structural bonding state, mortar disjoint, material freeze–thaw deterioration, and forced deformation of the foundation under extreme temperature conditions. Then, based on the principle of the beam-sheet plate, and considering the deterioration of ballastless track materials, the structural reinforcement in severely cold areas is checked and calculated. The stress state and damage characteristics of ballastless track structures in areas subject to seasonal freezing are revealed.

2. Finite Element Model of Ballastless Track

Ballastless track systems primarily consist of rails, fasteners, track slab, CA mortar layer, gel resin, a limit stop and baseplate, etc. [13,14]. Vertical and transverse fasteners adopt linear spring elements, while longitudinal fasteners adopt nonlinear spring elements. CRTS I type ballastless track fastener systems adopt the WJ-7B type normal resistance fastener; the lateral stiffness of the fastener system is 3.5×10^7 N/m, and vertical stiffness is 5×10^7 N/m. The longitudinal deformation resistance values of the fastener are shown in Formula (1) [15]:

$$r = \begin{cases} 12.0x & x \leq 2 \text{ mm} \\ 24.0 & x > 2 \text{ mm} \end{cases} \quad (1)$$

where r is the longitudinal resistance of the fastener (kN), and x is the longitudinal relative displacement between the rail and the rail bearing platform (mm).

The rail is equivalent to a Euler beam, which is supported by an elastic point and simulated by means of a beam188-type element; a combin14-type element is adopted for

the fastener, and the track structures and subgrade are simulated by means of a solid45-type element. The finite element model, consisting of 145,356 nodes and 54,508 elements, is shown in Figure 1.

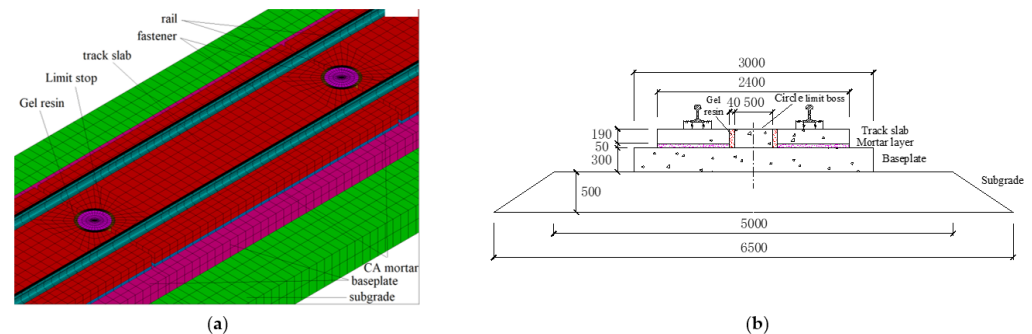


Figure 1. CRTS I ballastless track: (a) finite element model; (b) cross-section of track structure (unit: mm).

The rail linear expansion coefficient is $1.18 \times 10^{-5}/^{\circ}\text{C}$, and the concrete linear expansion coefficient is $1.0 \times 10^{-5}/^{\circ}\text{C}$. The parameters of the ballastless track system are shown in Table 1.

Table 1. Structural parameters of the ballastless track.

Structure	Poisson's Ratio	Elastic Modulus (GPa)	Density (kg/m^3)	Remarks
Rail	0.3	210	7800	CHN60
Track slab	0.2	36.0	2500	C60 grade concrete
Limit boss	0.2	32.5	2500	C40 grade concrete
Gel resin	-	0.02	1100	excellent bonding performance
CA mortar layer	0.15	0.30	2000	low temperature sensitivity
Baseplate	0.2	32.5	2500	C40 grade concrete
Subgrade	-	0.12	2000	surface stiffness $76 \text{ MPa} \cdot \text{m}^{-1}$
Bridge	0.2	32.5	2500	C40 grade concrete

3. Extreme Temperature Bonding Action

3.1. Temperature Load Mode

Temperature load is mainly divided into overall temperature load, temperature gradient load and concrete shrinkage and creep. The main structure of the ballastless track is made of concrete material, which is highly sensitive to temperature. Due to the differences in the material properties of the vertical layered structure of the track, the influence of the vertical temperature gradient load is the most significant.

Ballastless tracks are long strip structures with small contact surfaces between the sides and the air, which only affects the structural corners of the ballastless track. The temperature field model of a ballastless track can be simplified into a vertical one-dimensional linear heat transfer model, expressed as follows:

$$\frac{\partial T}{\partial t} = \zeta \frac{\partial^2 T}{\partial z^2} \quad (2)$$

where T is the temperature; t is the time; ζ is the thermal conductivity coefficient; z is the distance from the top surface of the structure.

Then, adopting the third type of boundary condition in heat conduction theory:

$$-\lambda \frac{\partial T_b}{\partial z} = B \left(T_a + \frac{Q_I}{B} - T_b \right) \quad (3)$$

where T_b is the atmospheric temperature; Q_J is the net radiation of the ballastless track; B is the heat release coefficient of the road surface, taken to be $B = 5.7 + 4v$; and v is the daily average wind speed; λ is the thermal conductivity of the concrete material.

The boundary temperature T_a of the track structure is:

$$T_a = T_1 + T_2[0.96 \sin(\omega(t - t_0)) + 0.14 \sin(2\omega(t - t_0))] \quad (4)$$

where T_1 is the daily average temperature; T_2 is the daily average increase; t_0 is the initial phase, usually taken to be 9; and ω is the internal angular frequency of one day.

Taking the climate parameters of the ballastless track structure in typical regions of China as an example, the meteorological data of Harbin in regions characterized by severe cold were selected, and the time history curve of vertical temperature load change in ballastless track slab structure within the annual range was obtained by solving the above equations, as shown in Figure 2.

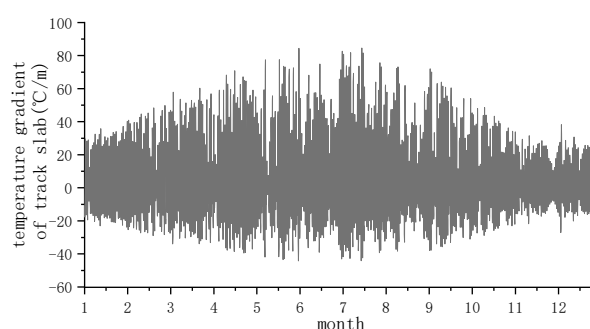


Figure 2. Time-history of vertical temperature gradient load on a track slab in Harbin.

The reliability of the temperature gradient load can be verified on the basis of a comparison with the relevant literature [16] and the code for design of highway cement concrete pavement [17]. There are many studies providing a relatively complete analysis and discussion of the mechanical properties of track structures under single temperature gradient loads. Considering extreme temperature load conditions, the negative temperature gradient load is taken to be $-50\text{ }^{\circ}\text{C/m}$, and the overall temperature load of the track slab is taken to be $-5\text{ }^{\circ}\text{C}$ for temperature superposition, that is, when the negative temperature gradient load is taken, the temperature of the track slab bottom is $0\text{ }^{\circ}\text{C}$, decreasing linearly to $-10\text{ }^{\circ}\text{C}$ at the track slab surface.

Under the action of a negative temperature gradient load, the dead weight is not able to completely restrain the temperature warping deformation of the track slab, resulting in poor contact between the track slab and the mortar cushion, local voids, and uneven stress. Under the action of train load, a “slap” effect will be produced, which will lead to mortar separation and damage. Under the action of a negative temperature gradient, the maximum longitudinal stress of the track slab will occur at the lower surface of both sides, and the maximum transverse stress will occur at the junction of the track slab and the lower surface of the limit stop. When studying the temperature load effect, it is necessary to consider the bonding state of the track slab and the mortar layer, which can be divided into two states: good bonding and poor bonding. Good bonding means that the mortar cushion was constructed using the formwork method, while poor bonding means that the mortar cushion was constructed using the bagging method. The interface transmits the vertical and horizontal temperature force through friction, and the friction coefficient is taken to be 0.3 [18]. The elastic moduli (E_{CA}) of 20, 50, 100, 200, 300, 500, 1000, 5000, 10,000 and 32,500 MPa were taken for the mortar material, respectively.

3.2. Mortar Layer under Track Slab with Good Bonding

The warping deformation trend of the track slab under negative temperature load is constrained by the bonding of the lower layer of mortar, and the mortar layer structure will

be subject to large warping stress during the subsequent forced deformation. The warping displacement of the track slab is shown in Figure 3.

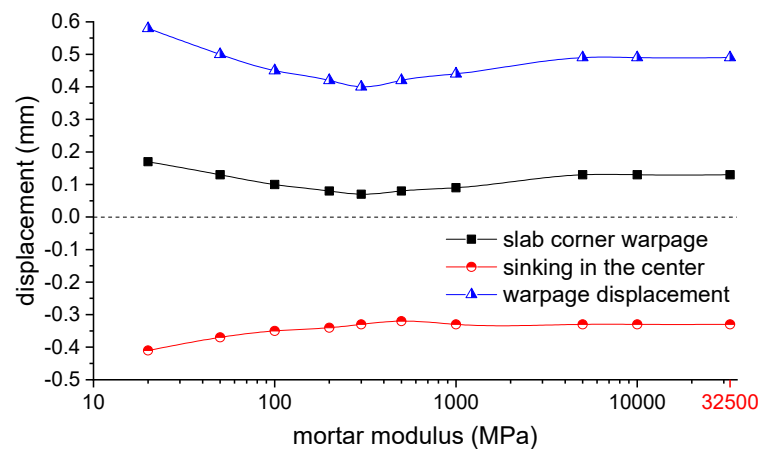


Figure 3. Warping displacement of track slab (with bonding).

As can be seen in Figure 3, with increasing mortar modulus, the warping displacement of the track slab decreases continuously, and a good constraint effect occurs when the elastic modulus of the mortar is 300 MPa. When the elastic modulus of the mortar increases to 5000 MPa, the displacement of track slab tends to be stable.

The warping stress of the track structure under each mortar elastic modulus is shown in Figure 4.

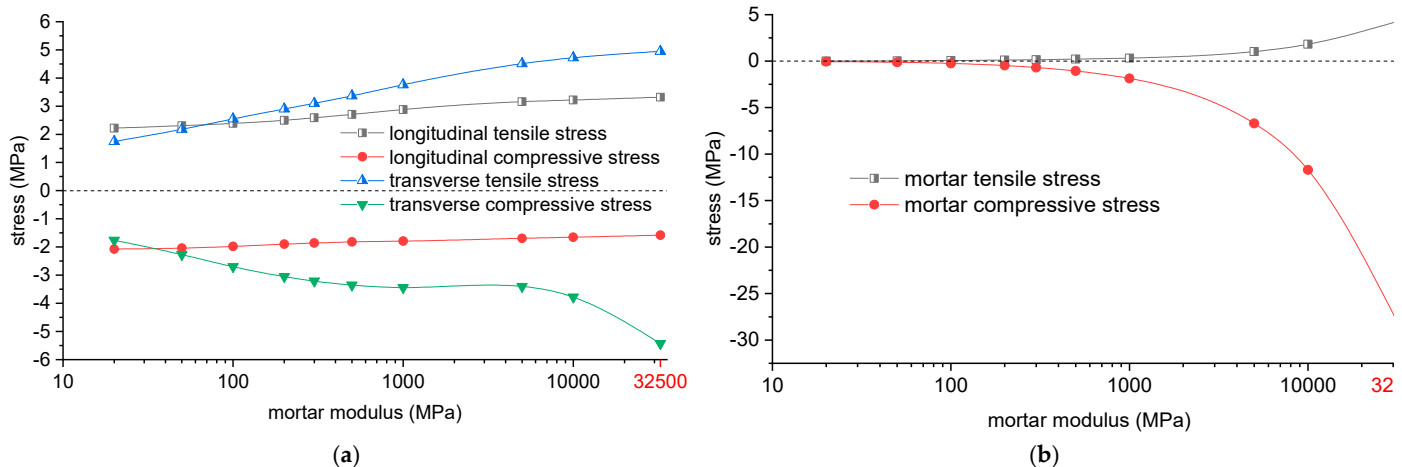


Figure 4. Warping stress of track structures (with bonding): (a) track slab; (b) CA mortar layer.

As can be seen from Figure 4, with the increase in the elastic modulus of the mortar, the extreme values of longitudinal and transverse tensile stress and transverse compressive stress at the edge of the track slab under the negative temperature gradient load continue to increase, while the maximum longitudinal compressive stress continues to decrease, such that the structural separation joint often appears at the side. As the limiting effect of the mortar layer on the warping deformation of the track board is gradually strengthened, the tensile and compressive stresses in the track board increase, which also results in higher compressive and tensile strengths for mortars with high elastic modulus, especially with regard to the bond strength between the track slab and the mortar cushion at the corner of the track slab.

3.3. Mortar Layer under Track Slab with Poor Bonding

The warping displacement and stress of the track structure under a negative temperature load are shown in Figure 5.

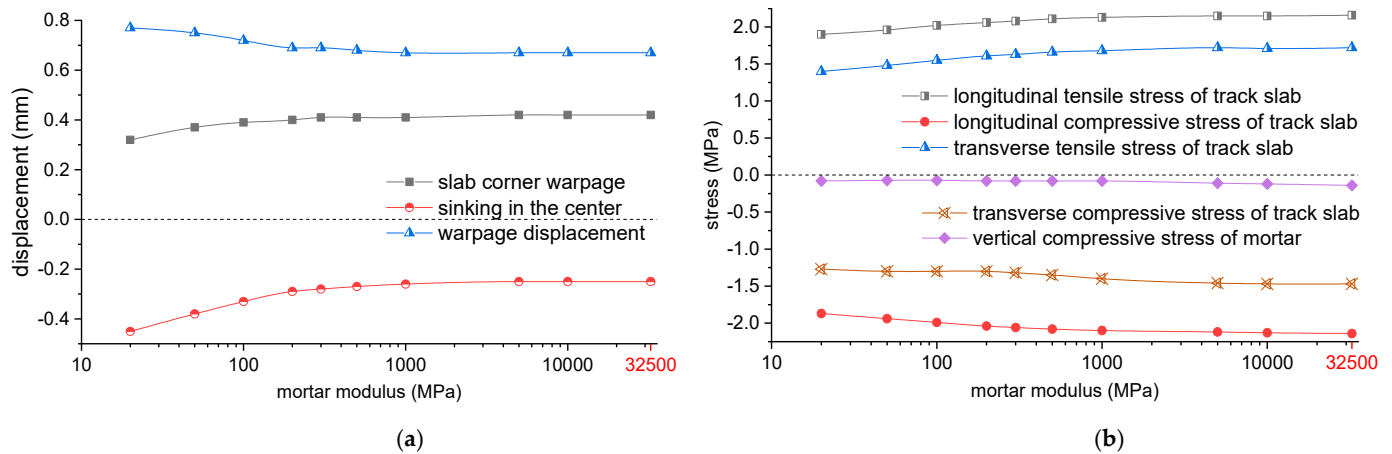


Figure 5. Warpage characteristics of structure (without bonding): (a) displacement of track structures; (b) stress of track structures.

Compared with the warping state with good bonding, the loss of bonding force is not conducive to the mortar layer restraining the upwarping deformation at the corner of the track slab; therefore, joint damage can easily develop on the four sides. At this time, the support of the mortar to the track slab is limited to the middle of the track slab. With the increase in the elastic modulus of the mortar, the bearing area decreases, and the overall state of the structure is worse than in the case where good bonding was used. The mortar cushion at the corner of the slab is subjected to cycles of high tensile and compressive stress. With increasing numbers of loading actions, the bond between the mortar and the track slab at the corner of the track slab will be destroyed first, meaning that it cannot guarantee the follow-up and restraint ability of the mortar regarding the warping deformation of the track slab.

In addition to the temperature gradient, the overall temperature difference with the lower foundation is also formed during the temperature change in the track slab [19]. It is difficult to maintain a permanent bonding state between the bottom of the track slab and the mortar. The ballastless track slab (or track bed slab) unit and the baseplate (or bearing layer) under it should be considered as a separate double-layer structure. The layer can only transmit limited horizontal force through friction. The calculation of warping displacement and stress is recommended in order to be able to take the absence of bonding between the two into consideration.

4. Subgrade Freeze–Thaw and Frost Heave Effect

The CRTS I slab ballastless track system, as the main track type used for high-speed railways in areas subject to severe cold, is directly exposed to the harsh environment. Under the influence of extreme climates and train loads, a series of deformations appear in the track slab, the cushion under the slab, the baseplate, and other components, such as cracking of the track slab, the track slab cushion, and the baseplate, the track slab separation, the appearance of voids at the bottom of the slab, and surface peeling of concrete material, and the reduction status of concrete material performance remains unclear.

4.1. Freeze–Thaw Cycle Test

With increasing operation time, rain seeps into the cracks and separation joints. Under the action of the freeze–thaw cycle and the dynamic load of the train, the concrete cracks and separation joints continue to evolve and develop. At the same time, the dynamic load

of the void part causes the track slab to repeatedly “beat” against the filling layer, further aggravating the damage to the filling layer or the track slab.

The track slab, the mortar layer, and the baseplate in the CRTS I slab ballastless track system are greatly affected by freeze–thaw cycles under environments characterized by seasonal freezing and cold temperatures. Therefore, the materials using in the test include C60 concrete for the track slab, C40 concrete for the baseplate, and cement-emulsified asphalt mortar materials for the filling layers.

C60 concrete material (group HT), C40 concrete material (group LT), and cement emulsified asphalt mortar material were used to produce standard cube test pieces with dimensions (length \times width \times height) of 150 mm \times 150 mm \times 150 mm. In addition, by successively pouring C60 concrete and mortar filling materials into the cube mold, a cube specimen (group OT) containing a bonding interface between the two materials was made to simulate the bonding interface between the track slab and the CA mortar layer, as shown in Figure 6. All specimens underwent 28 days of standard curing before testing.

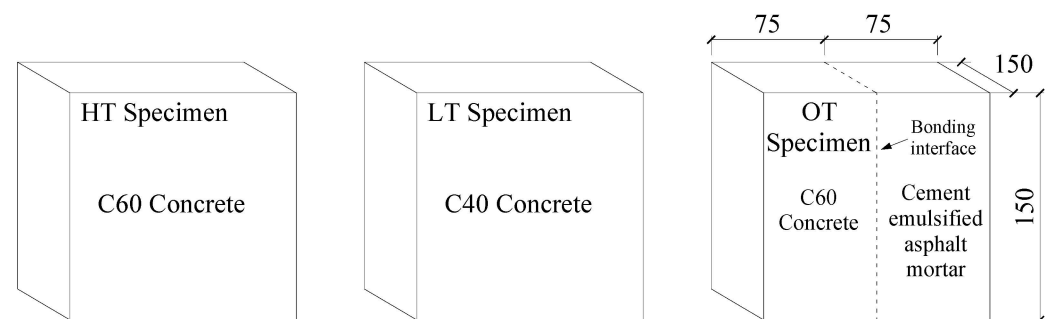


Figure 6. Schematic diagram of specimen preparation.

According to *Standard for Test Methods of Long-term Performance and Durability of Ordinary Concrete (GB/T50082-2009)*, the frost resistance grade of concrete is determined on the basis of multiple groups of parallel freeze–thaw cycles, with number of cycles N of 50, 100, 150, 200, 250 and 300, respectively. According to the statistical analysis, the corresponding numbers of outdoor freeze–thaw years are 0, 7.7, 25.4, 23.1, 30.8, 38.5 and 46.2 years [20]. The relationship between the peak compressive strength, axial tensile strength, and the number of freeze–thaw cycles in each group of specimens under the action of freeze–thaw cycles is shown in Figure 7. The peak strength is the axial compressive stress under the corresponding limit load, and the splitting tensile strength was converted according to the *Code for Design of Concrete Structures (GB50010-2010)* [21].

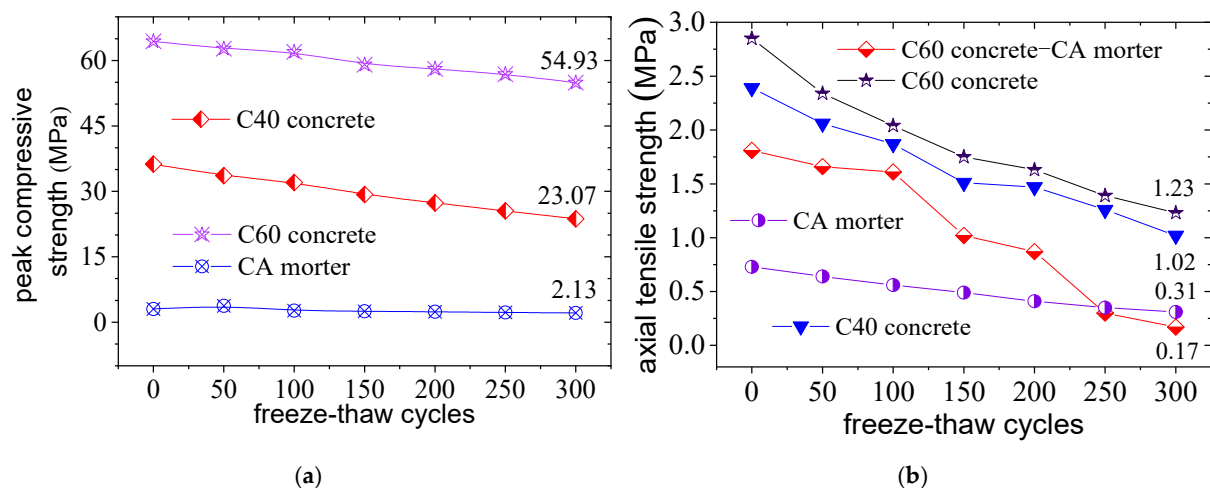


Figure 7. Strength curve of specimens: (a) axial compression failure test; (b) splitting tensile failure test.

It can be seen in Figure 7 that:

(1) With the intensification of the freeze–thaw cycle, the material properties of the specimen deteriorated significantly, and the compressive peak strength decreased significantly. For the ballastless track subjected to freeze–thaw cycles, the material performance was seriously deteriorated, and the main limiting structure was the mortar layer and concrete baseplate structure.

(2) With the increasing numbers of freeze–thaw cycles, the axial tensile strength of the material decreased significantly. More specifically, the maximum drop of cube specimen (C60 concrete–mortar) with cementation interface before and after freezing and thawing was more than 90%, the separation between the track slab structure and the mortar layer increased, and the tensile properties of C40 concrete structure were significantly affected.

The mechanical performance parameters of ballastless tracks consisting of various structural materials under different numbers of freeze–thaw cycles in indoor test are shown in Table 2.

Table 2. Mechanical parameters of materials under different freeze–thaw cycles.

Number of Cycles N	Material Number	Friction Coefficient	C60 Concrete (HT Test Piece)			CA Mortar			C40 Concrete (LT Test Piece)		
			E (GPa)	u	f_{tk} (MPa)	E (GPa)	u	f_{tk} (MPa)	E (GPa)	u	f_{tk} (MPa)
300	1	0.04	33.8	0.13	1.23	0.14	0.09	0.31	13.14	0.13	1.02
	2	0.19	34.9	0.165	2.04	0.245	0.12	0.52	19.59	0.15	1.48
	3	0.35	36	0.2	2.85	0.35	0.15	0.73	26.04	0.18	1.93
	4	0.5	-	-	-	-	-	-	32.5	0.2	2.39
250	1	0.08	34.27	0.14	1.39	0.15	0.10	0.35	13.96	0.14	1.26
	2	0.22	35.14	0.17	2.12	0.25	0.125	0.54	20.14	0.16	1.64
	3	0.36	36	0.2	2.85	0.35	0.15	0.73	26.32	0.18	2.01
	4	0.5	-	-	-	-	-	-	32.5	0.2	2.39
200	1	0.24	34.81	0.15	1.63	0.18	0.11	0.41	16.44	0.15	1.47
	2	0.33	35.41	0.175	2.24	0.265	0.13	0.57	21.79	0.17	1.78
	3	0.41	36	0.2	2.85	0.35	0.15	0.73	27.15	0.18	2.08
	4	0.5	-	-	-	-	-	-	32.5	0.2	2.39
150	1	0.28	35.23	0.16	1.75	0.19	0.12	0.49	17.31	0.16	1.51
	2	0.35	35.62	0.18	2.30	0.27	0.135	0.61	22.37	0.17	1.80
	3	0.43	36	0.2	2.85	0.35	0.15	0.73	27.44	0.19	2.10
	4	0.5	-	-	-	-	-	-	32.5	0.2	2.39
100	1	0.44	35.55	0.18	2.04	0.20	0.13	0.56	18.61	0.18	1.87
	2	0.46	35.78	0.19	2.445	0.275	0.14	0.645	23.24	0.187	2.04
	3	0.48	36	0.2	2.85	0.35	0.15	0.73	27.87	0.193	2.22
	4	0.5	-	-	-	-	-	-	32.5	0.2	2.39
50	1	0.46	35.76	0.19	2.34	0.22	0.14	0.64	20.18	0.19	2.06
	2	0.47	35.88	0.195	2.595	0.285	0.145	0.685	24.29	0.193	2.17
	3	0.49	36	0.2	2.85	0.35	0.15	0.73	28.39	0.197	2.28
	4	0.5	-	-	-	-	-	-	32.5	0.2	2.39
0	-	0.5	36	0.2	2.85	0.35	0.15	0.73	32.5	0.2	2.39

Note: f_{tk} is the axial tensile strength of the corresponding material; “-” indicates no data.

4.2. Combined Temperature Load

The rapid indoor freeze–thaw cycle test showed that the durability of the concrete baseplate structure and the mortar layer under repeated freeze–thaw cycles was greatly reduced, and the material performance reduction led to the uneven stress of the track structure. In the simulation model of the CRTS I slab ballastless track, the nature of the contact relationship between track layers is considered to be rigid, with a friction coefficient of 0.5 [13,22–24], and the contact interface between the surface layer of subgrade bed and the baseplate is taken to be the vertical boundary condition. Based on the actual continuous monitoring results of subgrade frost heave on site [25], the classic single-wave cosine curve representing the irregularity of the ballastless track and the frost heave deformation of the high-speed railway subgrade bed was used to simulate the basic waveform of subgrade frost heave, and the temperature load coupled with the frost heave load was then applied to the center of the baseplate (position a) and the expansion joint of the baseplate (position b).

(1) Track slab–CAM layer separation

When the temperature gradient load and subgrade frost heave act together, the void and separation state of the track slab and the CAM layer structure is slightly different from that in the case of the single frost heave load, as shown in Figure 8.

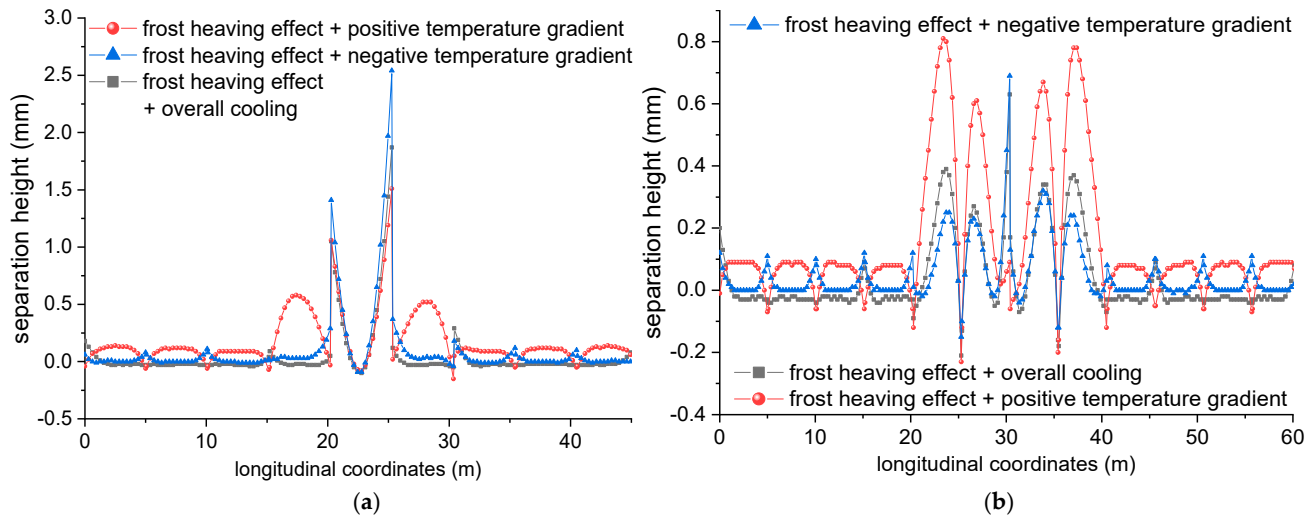


Figure 8. Effect of temperature combined load on track slab–CAM layer separation: (a) position a; (b) position b.

As can be seen in Figure 8, when frost heave acts at position a, the maximum separation under the slab is about 2.6 mm, which occurs at the end of the track slab under the load combination of “negative temperature gradient + frost heave effect”. When frost heave acts at position b, the maximum separation under the slab is about 0.8 mm, which occurs at the end of two track slabs under the load combination of “positive temperature gradient + frost heave effect”.

(2) Baseplate–subgrade separation

The separation between the baseplate and the surface structure of the subgrade bed is shown in Figure 9.

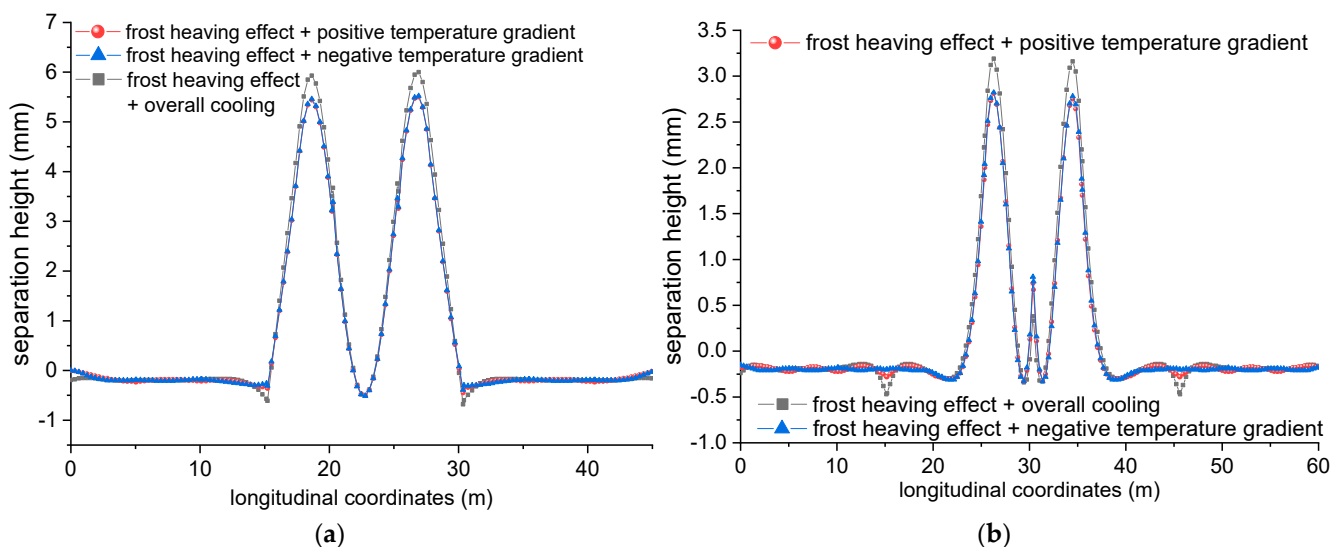


Figure 9. Effect of temperature combined load on baseplate–subgrade separation: (a) position a; (b) position b.

As can be seen from Figure 9, the separation law between the baseplate and the surface layer of the subgrade bed under the combined temperature load is similar to that under the

single load of subgrade frost heave. Under the combined load of “overall cooling + frost heave effect”, the maximum separation value is 5.9 mm when frost heave acts at position a, and 3.3 mm when frost heave acts at position b.

When frost heave acts at position a, the track structure bears the maximum stress under the load combination of “negative temperature gradient + frost heave effect”, and the stress in the middle of the upper surface of the track slab reaches 3.94 MPa. The temperature gradient load only acts on the track slab structure, and has little impact on the baseplate. The baseplate structure is mainly subject to the clamping deformation of frost expansion. The maximum stress under the load combination of “negative temperature gradient + frost heave effect” when frost heave acts at position b is 6.13 MPa.

In conclusion, taking into account the stress of the typical track structure and the interlayer separation, the load combination of “negative temperature gradient + frost heave effect” is the most unfavorable working condition, and the baseplate is a force-limiting structure.

4.3. CA Mortar Separation

In this section, the influence of mortar separation conditions and the most unfavorable mortar separation on the stress of the CRTS I slab ballastless track structure is discussed. Considering extreme damage conditions for the transverse through separation, the fastener spacing is taken as the longitudinal unit parting length, and the separation condition is shown in Figure 10. Of these, the frost heave separation condition in the slab refers to the separation of the two ends of the track slab at the center of the frost heave under the working conditions of the slab joint subjected to frost heave; and separation joint refers to the separation joint at the end of the track slab adjacent to the frost heave center. When frost heave acts at the center of the baseplate, there are separation joints at both ends of the track slab, located at the center of the frost heave. When frost heave acts at the expansion joint of the baseplate, there are separation joints at the ends of two adjacent track slabs at the center of the frost heave.

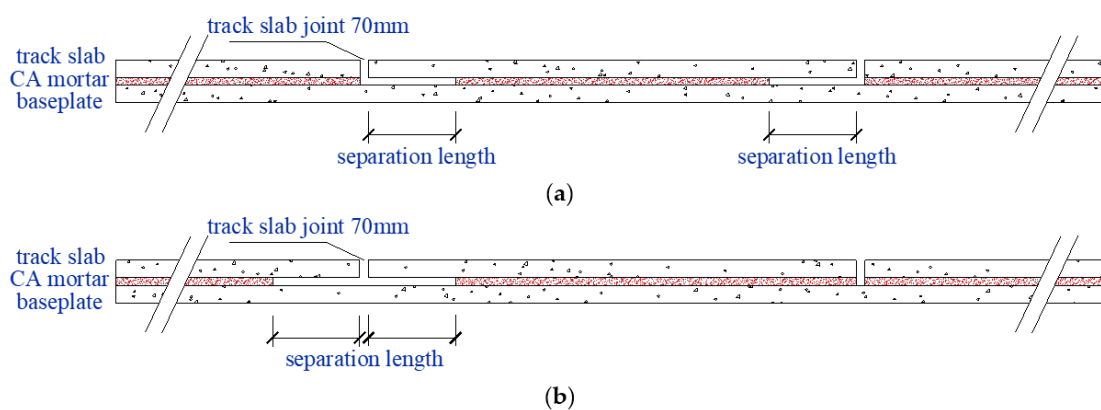


Figure 10. Schematic diagram of CAM separation: (a) frost heave acting at the center of the baseplate; (b) frost heave acting at the expansion joint of the baseplate.

Numerical simulations were performed using longitudinal separation distances of 0 m, 1×0.625 m, 2×0.625 m and 3×0.625 m and vertical separation distances of 0 mm, 2 mm, 6 mm, 10 mm and 15 mm, respectively. Taking frost heave acting at the expansion joint of the baseplate as an example, the extreme stress of each structure in the ballastless track system changes with the combination of separation conditions, as shown in Figure 11.

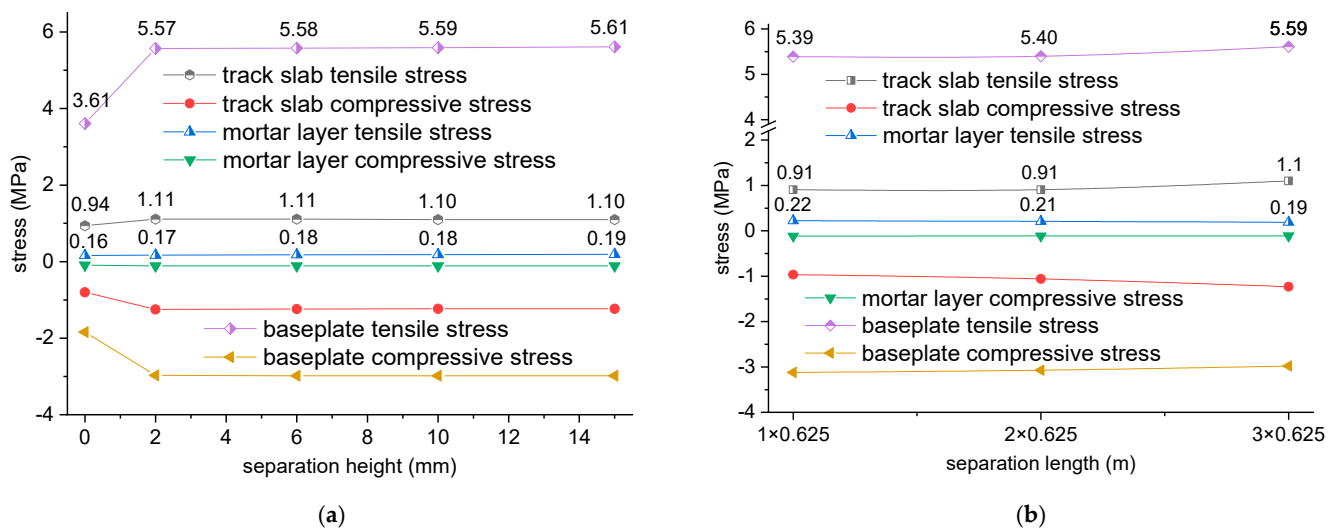


Figure 11. Extreme stress of track structure with CAM separation: (a) separation length 3×0.625 m; (b) separation height 15 mm.

For frost heave acting at the expansion joint of the baseplate, it can be seen in Figure 11a that when the fixed separation distance is 3×0.625 m, the extreme tensile stress of the track slab, mortar layer and baseplate structure increases with the increase in mortar separation distance, with the most unfavorable separation distance being 15 mm. Accordingly, when the fixed separation is 15 mm, as shown in Figure 11b, the extreme tensile stress of the track structure increases with the increase in the distance of mortar separation. The most unfavorable combination of separation conditions when frost heave acts at the expansion joint of the baseplate is the longitudinal separation distance of 3×0.625 m and the vertical separation distance of 15 mm. In the same way, for frost heave acting at the center of the baseplate, the most unfavorable combination of separation conditions is 3×0.625 m longitudinally and 2 mm vertically.

The end face of the ballastless track is affected by freezing and thawing, and the performance parameters of the concrete materials are greatly reduced within the range of the freezing and thawing depth [26]. The degree of deterioration gradually decreases from the surface to the interior. When the freezing and thawing depth of the concrete is exceeded, the concrete is no longer affected by freezing and thawing. According to the material parameters of the ballastless track structure in Table 2, considering the deterioration of the material following 300 freeze–thaw cycles, we calculated the impact of the most unfavorable mortar separation condition on the ballastless track, and the structural stress state is shown in Figure 12.

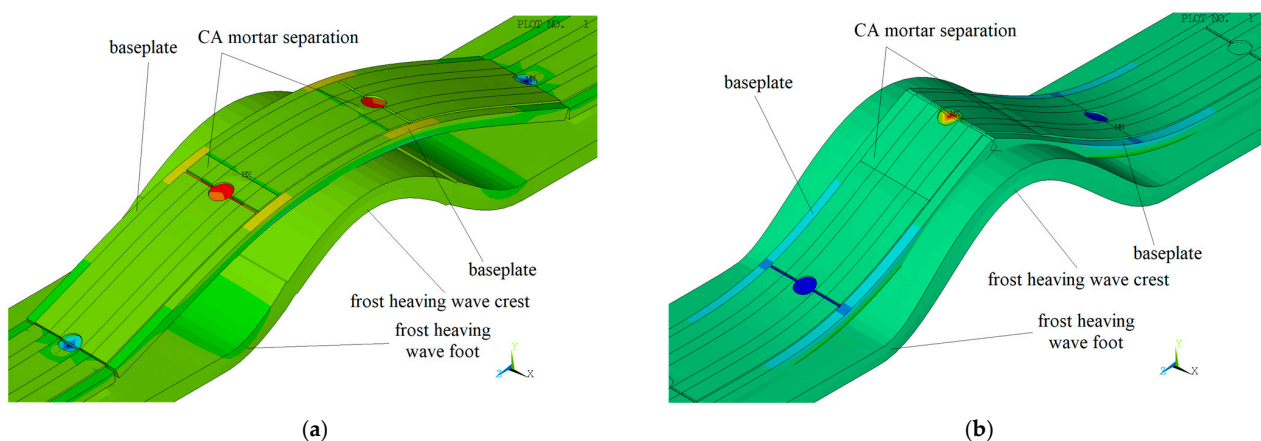


Figure 12. Stress nephogram of track structure under CAM separation damage (unit: Pa): (a) plate

seam frost heave seam release length 3×0.625 m; (b) plate seam frost heave seam release height 15 mm.

The structural stress of the baseplate under the freeze–thaw and frost heave load seriously exceeds the limit when separation is occurring under the plate. The mortar layer and the baseplate structure are weak limit structures. The most unfavorable frost heave condition changes to frost heave acting at the expansion joint of the baseplate, and the baseplate is the main load-bearing structure, with a maximum tensile stress of 6.38 MPa.

5. Reinforcement of Ballastless Track

The length of the concrete ballastless track slab in the horizontal direction is far greater than its vertical thickness, and its vertical deformation under the action of external load is far smaller than its own structural thickness. Therefore, the track slab (or track bed slab, or track bed) and the baseplate (or base, or support layer) can be regarded as an elastic thin plate structure, which is applicable to the plate and shell theory in finite element analysis. The slender rail structure can be regarded as a Euler beam structure that is suitable for the application of beam theory in finite element analysis. Faster systems, elastic damping layers and different lower elastic support foundations can be regarded as elastic structures of equivalent stiffness, for which spring theory in finite element analysis is applicable. In summary, the main structures of the ballastless track system together theoretically constitute an elastic foundation beam–plate–plate. Taking the ballastless track on a bridge as an example, the calculation model is shown in Figure 13.

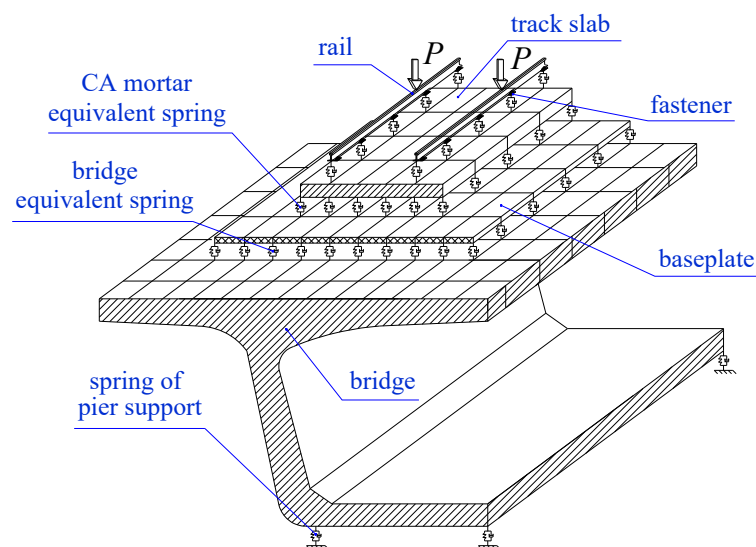


Figure 13. Elastic beam–plate of ballastless track slab on a bridge.

5.1. Theoretical Calculation of the Bending Moment of the Track Structure

The material parameters of the ballastless track system are shown in Table 1. The vertical supporting action of the lower supporting foundation structure (such as the subgrade, bridge and tunnel) is simulated using a continuous and uniform linear spring using different values of supporting stiffness, making the Winkler foundation assumption applicable. When the ballastless track is located in the subgrade section and the thickness of the surface layer of the subgrade bed is 0.5 m, the foundation coefficient is taken to be 76 MPa/m. When the ballastless track is located in the bridge and tunnel section, the foundation coefficient is taken to be 1000 MPa/m [18].

The elastic damping mortar layer structure is simulated using a continuous uniformly distributed linear spring, and the bearing stiffness k_1 of the spring surface of the mortar layer is calculated according to the “elastic modulus of the mortar layer/thickness of the

mortar layer". Considering that the supporting effect of the lower baseplate structure has a certain impact on the mortar elasticity, the baseplate elasticity needs to be included. The baseplate spring surface bearing stiffness k_2 is calculated according to the "baseplate elastic modulus/baseplate thickness". Finally, the total surface bearing stiffness k of the mortar layer (thin shell cushion layer) is calculated according to the series spring relationship, as shown in Formula (5):

$$1/k_m = \sum (1/k_1 + 1/k_2) \quad (5)$$

where k_1 is the stiffness of the mortar layer ($\text{MPa} \cdot \text{m}^{-1}$), k_2 is the stiffness of the baseplate ($\text{MPa} \cdot \text{m}^{-1}$), and k_m mortar is the total stiffness of the mortar layer support ($\text{MPa} \cdot \text{m}^{-1}$).

In order to avoid the calculation not possessing sufficient accuracy, when the spring element is used to support the elastic point of the plate and shell element, the structural mesh size of the shell element of the track slab and the baseplate should be 0.17 m~0.24 m, and the ratio of the long side to the short side of each element should be less than 1.5 [18].

5.2. Key Structural Load Parameters

The track structure design using the railway track limit state method, considering the load component coefficient, is based on the calculation of the force and deformation of the track structure under different loads and working conditions, and different combinations of loads are used to obtain the most unfavorable situation, and structural reinforcement design and crack width detection are carried out. In addition to the train load, temperature load, shrinkage deformation of concrete and other load factors mainly considered in the structural design of ballastless tracks in subgrade sections, and the impact of bridge deflection deformation should also be included for the bridge section.

(1) Train load

According to the *Design Code for High-Speed Railway*, the train load values are as follows [27]:

① Vertical design load:

$$P_d = \alpha \cdot P_j \quad (6)$$

where P_d is the vertical design load (kN) and P_j is the static wheel load (kN). α is the dynamic load coefficient, which is 3.0 for lines with design speeds of 300 km/h and above, and 2.5 for lines with design speeds of 250 km/h.

② Vertical fatigue check load:

$$P_f = 1.5 \cdot P_j \quad (7)$$

where P_f is the vertical design load (kN) and P_j is the static wheel load (kN).

The value of the train load is shown in Table 3:

Table 3. Train load value.

Train Load	Speed 350 km/h
Static axle load	17 t
Vertical design load	255 kN
Vertical fatigue check load	127.5 kN

③ Partial load coefficient (curve superelevation section):

Considering the partial load effect of the curve superelevation section, the decomposition diagram of the curve superelevation section is shown in Figure 14.

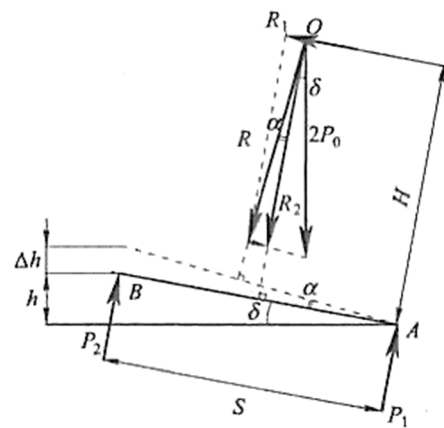


Figure 14. Decomposition diagram of a curve under superelevation.

When the vehicle passes the curve, the unbalanced superelevation (under-superelevation/over-superelevation) will cause the dynamic load of the outer rail (or inner rail) to increase, and the ratio of its increment to the static wheel load is called the eccentric load coefficient β . If P_2 is the actual wheel load on the outer rail (or inner rail) and P_0 is the static wheel load, then:

$$\beta = \frac{\Delta P}{P_0} = \frac{P_2 - P_0}{P_0} \quad (8)$$

Taking under-superelevation as an example, the calculation formula of β is derived. In Figure 10, the actual superelevation of the track is h , and the unbalanced superelevation (under-elevation) is Δh . The included angle between the rail surface line and the horizontal line inside and outside the curve is δ , the included angle between the under-superelevation line and the rail surface line is α , the locomotive axle load is $2P_0$, the centrifugal force is J (not shown in Figure 10), and the combined force of the two is recorded as R . If R is decomposed into the force R_1 parallel to the rail surface line and the force R_2 perpendicular to the rail surface line, then:

$$\begin{cases} R = \frac{2P_0}{\cos(\alpha + \delta)} \\ R_1 = \frac{2P_0 \sin \alpha}{\cos(\alpha + \delta)} \\ R_2 = \frac{2P_0 \cos \alpha}{\cos(\alpha + \delta)} \end{cases} \quad (9)$$

If the reaction forces of the two rails are P_1 and P_2 , respectively, the sum of the moment at point A is as follows:

$$\sum M_A = P_2 S - R_2 \frac{S}{2} - R_1 H = 0 \quad (10)$$

where H is the distance from the vehicle center to the rail surface line, and S is the distance between the inner and outer rail center lines. Since the values of δ and α are very small, it can be approximated that:

$$\begin{cases} \cos(\alpha + \delta) = \cos \alpha = 1 \\ \sin \alpha = \frac{\Delta H}{S} \end{cases} \quad (11)$$

By substituting Formulas (9) and (11) into Formula (10), we can get:

$$P_2 = P_0 + \frac{2P_0 H \Delta h}{S^2} \quad (12)$$

$$\beta = \frac{P_2 - P_0}{P_0} = \frac{2H \Delta h}{S^2} \quad (13)$$

Take $H = 2300$ mm and $S = 1500$ mm; then, β_u can be expressed as a function of under-elevation Δh :

$$\beta_u = \frac{2 \times 2300 \times \Delta h}{1500^2} = 0.002 \Delta h \quad (14)$$

The actual wheel load of outer rail under superelevation β_2 (quasi-static method) is:

$$P_2 = (1 + \beta) \cdot P_0 \quad (15)$$

The over-superelevation can be calculated using the same principle; the superelevation of the baseplate in the curve section of the ballastless track is 80 mm, and the most unfavorable 90 mm is used for the calculation of under-superelevation/over-superelevation.

(2) Temperature gradient load

The stress and bending moment caused by the temperature gradient are calculated as follows:

$$\sigma = \frac{E\alpha_t\beta_h T_g h}{2} \quad (16)$$

$$M = \frac{bh^2}{6} \sigma \quad (17)$$

where T_g is the negative temperature gradient load, taken to be -50°C/m , σ is the temperature warping stress, M is the temperature warping moment, α_t is the linear expansion coefficient of concrete, taken to be 10^{-5} , β_h is the temperature gradient plate thickness correction factor, and h, b are the track structure thickness and width, respectively.

(3) Bridge deflection

According to the *Code for Design of High-speed Railway (TB10621-2014)*, the limit value of bridge deflection [27,28] should be taken to be as shown in Table 4.

Table 4. Vertical deflection limit of the bridge body.

Train Speed	Deflection Limit of Different Beam Spans		
	$L \leq 40 \text{ m}$	$40 \text{ m} < L \leq 80 \text{ m}$	$L > 80 \text{ m}$
300 km/h	$L/1500$	$L/1600$	$L/1100$
350 km/h	$L/1600$	$L/1900$	$L/1500$

The bridge deck bearing stiffness is large, and the rigid foundation method is adopted. The bending moment of the baseplate under the bridge deflection is:

$$M = EI\kappa_{\max} \quad (18)$$

$$\kappa_{\max} = \frac{\pi^2 \delta}{L^2} \quad (19)$$

where κ_{\max} is the maximum curvature of the foundation deformation, δ is the midspan deflection of the bridge (mm), determined according to the limit value of the bridge deflection-to-span ratio, and L is the bridge span (m).

5.3. Combination of Load Main Force

Main force combination 1: train design load, used for strength and crack checking.

Main force combination 2: train vertical fatigue check load + common temperature gradient + bridge deflection (not considered for subgrade section), used for strength and crack checking.

According to the provisions of *Code for Design of Railway Track (Limit State Method)* [29,30], the design value of the basic combined bending moment is determined according to Formula (20):

$$M \leq \gamma_d M_{dk} + \psi_{td} \gamma_{td} M_{tdk} + \gamma_{nq} M_{nqk} \quad (20)$$

where M_{dk} is the standard value of train load bending moment, the partial coefficient γ_d of the new high-speed railway is 1.5, M_{tdk} is the standard value of the bending moment under the temperature gradient, the combination coefficient $\psi_{td} = 0.5$, the partial coefficient

$\gamma_{td} = 1.0$, M_{nqk} is the standard value of bending moment under beam bending deformation, and the partial coefficient $\gamma_{nq} = 1.0$.

5.4. Checking the Calculation of Bending Moment Reinforcement

The material properties of steel bars and concrete determine their ability to work together. Due to steel bars and concrete sharing a similar linear expansion coefficient, excessive stress will not be generated due to different environments. There is a good bonding force between steel bars and concrete. By setting spaced ribs onto the surface of the steel bars, the mechanical engagement (i.e., longitudinal bonding force) between concrete and steel bars can be improved. Furthermore, when this is still insufficient to transmit the relative tension between the steel bars and the concrete, the end of the steel bars can be bent 180 degrees with a hook for reinforcement. It is worth mentioning that, due to the alkaline environment provided by calcium hydroxide in concrete, a passivation protective film is formed on the surface of the steel bars, making them less susceptible to corrosion compared to neutral and acidic environments.

The upper and lower layers of HRB335 reinforcement are set in the track slab and baseplate, the minimum reinforcement ratio is 0.15%, and the minimum net thickness of the protective layer of concrete in the ballastless track structure is 40 mm. The allowable value of surface crack width is 0.233 mm, and the allowable stress of the reinforcement is 176 MPa. The bending moments of track slab and baseplate of different supporting foundations (roadbeds, bridges) in straight and curved sections under the most unfavorable freeze–thaw cycle deterioration conditions were calculated, and the structural reinforcement in cold areas was calculated. When the train load in the subgrade section acts on the center of the slab, the longitudinal bending moment distribution of the structure is as shown in Figure 15.

According to the limit state method of bearing capacity, the combination of structural load bending moment values was performed according to Formula (20), and a summary of the results is shown in Tables 5 and 6. The reinforcement check settings are provided in Table 7.

Table 5. Bending moment of ballastless track structure in the subgrade section.

Load Combination	Structure	Line Type	Longitudinal		Transverse	
			Positive Bending Moment	Positive Bending Moment	Positive Bending Moment	Positive Bending Moment
Main force combination 1	Track slab	Straight section	14.20	3.86	16.89	6.82
		Curved section	11.20	17.17	16.34	26.39
	Base	Straight section	74.07	27.89	23.41	3.41
		Curved section	42.11	14.07	24.75	8.09
Main force combination 2	Track slab	Straight section	7.15	1.88	8.55	3.34
		Curved section	5.61	9.32	8.17	13.93
	Base	Straight section	37.67	14.93	12.70	0.02
		Curved section	7.55	8.05	15.10	25.19

It can be seen from Tables 5 and 6 that under the most unfavorable main force combination in the limit state of bearing capacity, the main structure of the ballastless track slab in the subgrade section, especially the base structure (block type), bears more significant bending moments than the bridge section. Compared with the non-freeze–thaw condition, the maximum increase in the stress of the longitudinal positive bending moment (longitudinal bottom reinforcement) in the superelevation section of the subgrade curve is 513%.

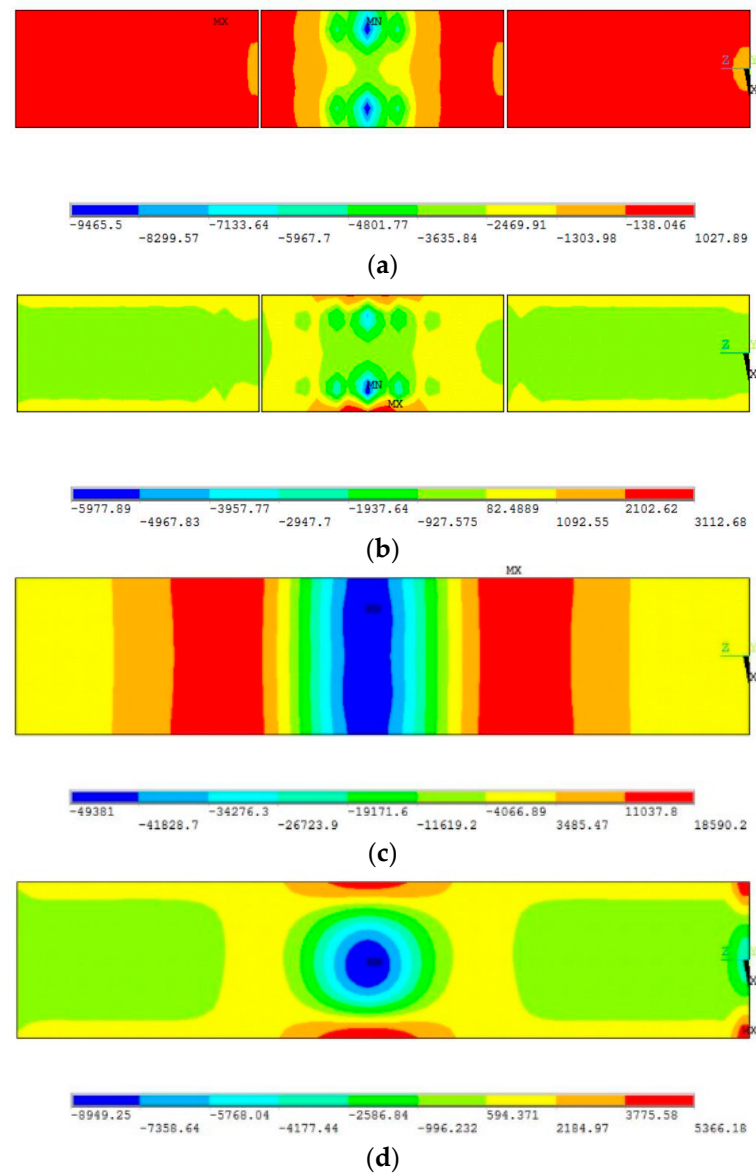


Figure 15. Longitudinal bending moment of the ballastless track structure (unit: N·m/m): (a) track slab—straight section; (b) track slab—curved section; (c) baseplate—straight section; (d) baseplate—curved section.

Table 6. Bending moment of ballastless track structure in bridge section.

Load Combination	Structure	Line Type	Longitudinal		Transverse	
			Positive Bending Moment	Positive Bending Moment	Positive Bending Moment	Positive Bending Moment
Main force combination 1	Track slab	Straight section	12.62	4.55	17.05	7.75
		Curved section	11.06	16.03	16.14	27.14
	Base	Straight section	12.08	4.07	10.58	7.30
		Curved section	6.29	14.33	10.54	23.37
Main force combination 2	Track slab	Straight section	10.26	6.12	12.50	7.18
		Curved section	9.43	12.39	11.94	17.97
	Base	Straight section	9.98	5.88	9.39	7.35
		Curved section	7.50	12.00	9.63	16.52

Table 7. Check and calculation of reinforcement of ballastless track slab.

Crack Limit		0.233 mm (HRB335)			Crack Limit		0.233 mm (HRB335)		
Rebar Position	Diameter (mm)	Reinforcement Ratio %	Area (mm ²)	Number of Reinforcement	Rebar Position	Diameter (mm)	Reinforcement Ratio %	Area (mm ²)	Number of Reinforcement
Longitudinal top design	16	30	1206	Original 6	Longitudinal top design	10	37/34	1571/1414	Original 20/18
Straight track slab of subgrade	16	30	1206	6	Straight base of subgrade	12(+2)	28	2262	20
Curved track slab of subgrade	16	50	2011	10(+4)	Curved base of subgrade	10	19	1571	20
Straight track slab of bridge	16	30	1206	6	Straight baseplate of bridge	10	34	1414	18
Curved track slab of bridge	16	50	2011	10(+4)	Curved baseplate of bridge	10	41	1728	22(+4)
Longitudinal bottom design	16	30	1206	Original 6	Longitudinal bottom design	10	37/34	1571/1414	Original 20/18
Straight track slab of subgrade	16	46	1810	9(+3)	Straight base of subgrade	16(+6)	65	5228	26(+6)
Curved track slab of subgrade	16	35	1407	7(+1)	Curved base of subgrade	12(+2)	39	3167	28(+8)
Straight track slab of bridge	16	40	1609	8(+2)	Straight baseplate of bridge	10	36	1492	19(+1)
Curved track slab of bridge	16	35	1407	7(+1)	Curved baseplate of bridge	10	34	1414	18
Transverse top design	16	44	3016	Original 15	Transverse top design	10	39	2827	Original 36
Straight track slab of subgrade	16	44	3016	15	Straight base of subgrade	10	39	2827	36
Curved track slab of subgrade	16	84	5831	29(+14)	Curved base of subgrade	10	39	2827	36
Straight track slab of bridge	16	44	3016	15	Straight baseplate of bridge	10	39	2827	36
Curved track slab of bridge	16	84	5831	29(+14)	Curved baseplate of bridge	12(+2)	64	4637	41(+5)
Transverse bottom design	16	44	3016	Original 15	Transverse bottom design	10	39	2827	Original 36
Straight track slab of subgrade	16	58	4021	20(+5)	Straight base of subgrade	10	23	2906	37(+1)
Curved track slab of subgrade	16	58	4021	20(+5)	Curved base of subgrade	10	25	3063	39(+3)
Straight track slab of bridge	16	58	4021	20(+5)	Straight baseplate of bridge	10	39	2827	36
Curved track slab of bridge	16	58	4021	20(+5)	Curved baseplate of bridge	10	39	2827	36

Note: The number of reinforcement layers in brackets is the increase or decrease. For the number of layers of base reinforcement, “A/B” refers to the subgrade section and “B” refers to the bridge section.

It can be seen from Table 7 that the original design of the substructure structure reinforcement is generally not able to meet the requirements imposed by structural cracks and the yield stress of the reinforcement, so it is necessary to increase the number of reinforcement layers or increase the diameter of the reinforcement. It is generally necessary to redesign the reinforcement for curve sections, and the maximum increase of five bars at the bottom of the track slab structure can meet the requirements of crack control. Similarly, the reinforcement at the bottom of the base structure is 12 mm in diameter, with a maximum increase of eight bars. Under the influence of freeze–thaw cycle deterioration in cold areas, structural optimization design was carried out conditioned upon meeting the minimum requirements regarding protective layer thickness and steel bar spacing; the specific steel bar inspection results can be found by referring to Table 7.

6. Conclusions

Taking the structure of ballastless track system in severe cold regions of China as the research object, a precise finite element model of the CRTS I type slab ballastless track was established, and the influence of the bonding state of the mortar layer under the track slab on structural stress was analyzed. Considering the damage of mortar separation under the effect of freeze–thaw deterioration, the damage law of the ballastless track under temperature load, foundation deformation and equal load was discussed. Finally, a beam–plate model of ballastless track system on bridge and subgrade was established to

check and calculate the reinforcement of the track structure. The main conclusions were as follows:

(1) When the interface between the track slab and the mortar layer is poorly bonded, the warping deformation of the track structure will increase. The structural stiffness of the mortar layer should be appropriately increased to improve the bearing capacity.

(2) The deterioration of the material properties under freeze–thaw cycles is serious, the phenomenon of separation between the track slab structure and the mortar layer intensifies, and the tensile properties of the baseplate structure are significantly affected. The maximum tensile stress of the baseplate under the coupling action of negative temperature gradient and foundation frost heave load exceeds 6 MPa.

(3) The mortar layer and the baseplate structure are weak limit structures when there are gaps under the track slab. The most unfavorable foundation deformation condition is frost heave acting at the expansion joint of the baseplate, which is the main load-bearing structure.

(4) Under the effect of freeze–thaw deterioration, the original reinforcement design of the substructure structure does not meet the requirements of structural cracks and the yield stress of the reinforcement. It is necessary to increase the number of reinforcement layers, or increase the diameter of the reinforcement, and it is necessary to redesign the structural reinforcement.

Author Contributions: Conceptualization, H.X. and L.X.; methodology, L.X. and B.Y.; software, H.X. and B.Y.; validation, B.Y. and L.X.; formal analysis, H.X. and B.Y.; writing—original draft preparation, H.X. and L.X.; writing—review and editing, B.Y., H.X. and L.X. All authors have read and agreed to the published version of the manuscript.

Funding: This research was funded by the National Natural Science Foundation of China (grant number 52278470), the Natural Science Foundation of Hunan Province (grant number 2022JJ30741), the Scientific and Technological R&D Program of China Railway (grant number K2020G025), the Scientific and Technological R&D Program of China Railway Design Corporation (grant number 2022A02036002).

Institutional Review Board Statement: Not applicable.

Informed Consent Statement: Not applicable.

Data Availability Statement: All data, models and code generated or used during the study appear in the submitted article.

Acknowledgments: The authors would like to thank the National Natural Science Foundation of China (grant number 52278470), the Natural Science Foundation of Hunan Province (grant number 2022JJ30741), the Scientific and Technological R&D Program of China Railway (grant number K2020G025), the Scientific and Technological R&D Program of China Railway Design Corporation (grant number 2022A02036002).

Conflicts of Interest: The authors declare no conflict of interest.

References

1. Zhang, P.-F.; Gui, H.; Gao, L.; Lei, X.-Y. Analysis on influencing factors of deflection force of CRTS II slab ballastless track on bridge. *J. Railw. Sci. Eng.* **2019**, *16*, 25–33. (In Chinese)
2. Yan, B.; Cheng, R.; Xie, H.; Zeng, Z.P. Mechanical characteristics of CRTS II ballastless track on bridge due to extreme temperature load. *J. Railw. Sci. Eng.* **2021**, *18*, 830–836. (In Chinese)
3. Chang, W.; Cai, X.; Luo, B.; Li, H.; Sun, J. Structure deformation and damage of ballastless track of roadbed-bridge transition section in severe cold region. *China Railw. Sci.* **2021**, *42*, 15–25. (In Chinese)
4. Feng, Q.; Liao, C.; Sun, K.; Lei, X. Influence of complex temperature load on ballastless track on continuous beam bridge. *J. Railw. Sci. Eng.* **2021**, *18*, 2280–2288. (In Chinese)
5. Zhang, P.; Tu, J.; Gui, H.; Lei, X.; Liu, L. Mechanical properties of CRTS II slab ballastless track on bridge under temperature gradient loads. *J. Southwest Jiaotong Univ.* **2021**, *56*, 945–952. (In Chinese)
6. Yang, R.; Li, J.; Kang, W.; Liu, X. Temperature characteristics analysis of the ballastless track under continuous hot weather. *J. Transp. Eng. A Syst.* **2017**, *143*, 04017048. [[CrossRef](#)]

7. Zhang, J.; Cai, C.; Zhu, S.; Wang, M.; He, Q.; Yang, S.; Zhai, W. Experimental investigation on dynamic performance evolution of double-block ballastless track under high-cycle train loads. *Eng. Struct.* **2022**, *254*, 113872. [[CrossRef](#)]
8. Xu, Q.; Sun, S.; Xu, Y.; Hu, C.; Chen, W.; Xu, L. Influence of temperature gradient of slab track on the dynamic responses of the train-CRTS III slab track on subgrade nonlinear coupled system. *Sci. Rep.* **2022**, *12*, 14638. [[CrossRef](#)]
9. Jiang, H.; Li, Y.; Wang, Y.; Yao, K.; Yao, Z.; Xue, Z.; Geng, X. Dynamic performance evaluation of ballastless track in high-speed railways under subgrade differential settlement. *Transp. Geotech.* **2022**, *33*, 100721. [[CrossRef](#)]
10. Zeng, Z.; Huang, Z.; Yin, H.; Meng, X.; Wang, W.; Wang, J. Influence of track line environment on the temperature field of a double-block ballastless track slab. *Adv. Mech. Eng.* **2018**, *10*, 1687814018812325. [[CrossRef](#)]
11. Dai, G.; Su, M. Mechanism of interfacial bond failure for slab ballastless track under shear loading. *J. Huazhong Univ. Sci. Technol. Nat. Sci. Ed.* **2016**, *44*, 16–21. (In Chinese)
12. Jiang, H.; Li, X.; Xin, G.; Yao, Z.; Zhang, J.; Liang, M. Geometry mapping and additional stresses of ballastless track structure caused by subgrade differential settlement under self-weight loads in high-speed railways. *Transp. Geotech.* **2019**, *18*, 103–110. [[CrossRef](#)]
13. Yan, B.; Xie, H.; Shen, Q.; Li, Z. Irregularity properties and stress characteristics of CRTS I ballastless track in seasonal frozen area. *J. Harbin Inst. Technol.* **2021**, *53*, 110–117. (In Chinese)
14. Cai, X.; Luo, B.; Chang, W.; Liang, Y. Research on deformation and damage of CRTSDI slab track in severe cold regions. *J. Huazhong Univ. Sci. Technol. Nat. Sci. Ed.* **2019**, *47*, 92–97. (In Chinese)
15. Feng, Q.-S.; Sun, K.; Xu, J.-H.; Lei, X.-Y. Study of Influence of the bridge temperature distribution conditions on ballastless track on bridge. *J. Railw. Eng. Soc.* **2018**, *35*, 20–26. (In Chinese)
16. Zhao, P.; Liu, X.; Yang, R.; Guo, L. Experimental study of temperature load determination method of bi-block ballastless track. *J. China Railw. Soc.* **2016**, *38*, 92–97. (In Chinese)
17. Chinese National Standards, JTG D40-2011; Code for design of Highway Cement Concrete Pavement. People's Communications Press: Beijing, China, 2011. (In Chinese)
18. Zhao, P. Research on the Design Theory and Method for Ballastless Track on Passenger Dedicated Line. Ph.D. Thesis, Southwest Jiaotong University, Chengdu, China, 2008. (In Chinese).
19. Yan, B.; Liu, S.; Dai, G.; Pu, H. Vertical nonlinear temperature distribution and temperature mode of unballasted track in typical areas of China. *J. China Railw. Soc.* **2016**, *38*, 81–86. (In Chinese)
20. Li, C.; Chen, S.; He, Z.; Gu, X. Analysis of concrete structure life under freezing thawing cycle conditions. *Eng. J. Wuhan Univ.* **2010**, *43*, 203–207. (In Chinese)
21. Chinese National Standards, GB 50010-2010; Code for Design of Concrete Structures. Ministry of Housing and Urban-Rural Development of the People's Republic of China: Beijing, China, 2010. (In Chinese)
22. Li, J. Study on the Influence for the CRTS I Slab Track Induced by Subgrade Frost Heaving. Master's Thesis, Southwest Jiaotong University, Chengdu, China, 2016. (In Chinese)
23. Zhao, G.; Zhao, L.; Zhang, L. Mechanical characteristics of ballastless track undersubgrade frost heaving in high-speed railway. *J. Railw. Eng. Soc.* **2017**, *34*, 53–61. (In Chinese)
24. Cai, X.; Liang, Y.; Tan, S.; Shen, Y. Deformation and seam characteristics analysis of CRTSI slab ballastless track in subgrade frost heaving zone. *J. Beijing Jiaotong Univ.* **2017**, *41*, 7–13. (In Chinese)
25. Zhao, G. Study on management standard of frost heaving of ballastless track subgrade on high-speed railway in severe cold regions. *J. China Railw. Soc.* **2016**, *38*, 1–8. (In Chinese)
26. Li, X.; Huang, X.; Zhang, D.; Xue, C. Properties of the concrete for the slab ballastless track of CRTS III. *Mater. Sci. Forum.* **2017**, *898*, 2071–2075. [[CrossRef](#)]
27. Chinese National Standards, TB 10621-2014; Code for Design of High Speed Railway. China Railway Publishing House: Beijing, China, 2014. (In Chinese)
28. de Oliveira, F.M.; Greco, M. Nonlinear dynamic analysis of beams with layered cross sections under moving masses. *J. Braz. Soc. Mech. Sci. Eng.* **2015**, *37*, 451–462. [[CrossRef](#)]
29. Chinese National Standards, TB/T 10082-2017; Code for Design of Railway Track. National Railway Administration of People's Republic: Beijing, China, 2017. (In Chinese)
30. Yamchelou, M.T.; Nikbin, I.M.; Zareian, H.; Charkhtab, S. Assessing Absolute Maximum Vibration Amplitude of a Rectangular Plate Subjected to a Moving Mass. *Iran. J. Sci. Technol. Trans. Civ. Eng.* **2017**, *41*, 135–147. [[CrossRef](#)]

Disclaimer/Publisher's Note: The statements, opinions and data contained in all publications are solely those of the individual author(s) and contributor(s) and not of MDPI and/or the editor(s). MDPI and/or the editor(s) disclaim responsibility for any injury to people or property resulting from any ideas, methods, instructions or products referred to in the content.